New Computational Methods for the Construction of "Darcyan" Biological Coordinate Systems

Nataliya Portman[1], Ulf Grenander[2], and Edward R. Vrscay[1]

[1]Department of Applied Mathematics, Faculty of Mathematics
University of Waterloo, Waterloo, Ontario, Canada N2L 3G1
[2]L. Herbert Balliou University Professor Emeritus
Division of Applied Mathematics, Brown University, Providence, RI, USA 02912
nportman@uwaterloo.ca,ulf-grenander@cox.net,ervrscay@uwaterloo.ca

Abstract. In this paper we pursue the goal of constructing a biologically meaningful coordinate system that (i) carries information about the spatial distribution of gene activity regions and (ii) captures its effect on the internal structure and shape of an organism during its growth. Geometrically, this "Darcyan" coordinate system is curvilinear and comprised of an interior grid surrounded by a closed curve, namely the boundary of the organism. We explore two computational methods of constructing it, one based on potential theory (Poisson equation) and the other based on level set methods, with particular emphasis placed on the latter. We propose a novel algorithm that uses image processing tools for the extraction of the boundary, from which is produced the interior Darcyan coordinate system by means of level set evolution. Examples show the ability of the proposed algorithm to handle the complex geometry of the initial boundary such as significant oscillations, corners and cusps.

1 Introduction

The motivation for the design of a biologically meaningful coordinate system within a multicellular organism comes from computational anatomy [7]. One of the ultimate goals of computational anatomy is to infer the type of development of biological tissue from a series of observations made during its growth (e.g., from medical images). It is difficult to detect pathologies that may affect the internal structure and shape of the developing organism simply from a visual inspection of images, especially if such pathologies exist at the very finest scale. In order to recognize normal or abnormal development patterns in observed images based on morphological changes, it is necessary to consider biological growth as a morphogenetic process. Only then can a comparison between individuals in healthy and diseased groups be performed in a biologically and quantitatively meaningful manner for the purpose of classification.

The concept of a biological coordinate system was introduced by U. Grenander [3,4] as a major ingredient of the genetically-based model of biological growth. In this paper, we briefly explain the notion of the biological coordinate system

M. Kamel and A. Campilho (Eds.): ICIAR 2007, LNCS 4633, pp. 143–156, 2007.

and develop two principal computational methods for the construction of such "Darcyan" coordinate systems.

The first method, offered by Grenander [3], is a modification of the inhomogeneous Thomas-Thames-Mastin elliptic grid generator [5]. The source term of the elliptic equation is assumed to have the form of a unit Dirac delta function. Given the domain of the organism with its boundary as determined from a 2D medical image, the elliptic technique generates one set of radial coordinate curves as the equipotential contours of the solution to Poisson's equation. The transverse curves to these radial coordinate curves are then constructed. A user's choice of the origin of the coordinate system provides flexibility in a grid construction, and a relatively uniform distribution of coordinate lines can be achieved but with a high computational cost. This major drawback of the elliptic approach is due to the slow speed of convergence.

The second method for 2D interior grid generation is based upon the level set method [8]. Using a Lagrangian approach, the method yields both radial and angular coordinate lines simultaneously by means of the inward flow of the initial boundary. The speed of the boundary propagation is a choice between the mean curvature or a threshold value. Such a speed function yields a smooth flow of the grid. Convergence of the angular coordinate lines to the origin of this coordinate system can be established by completing the curvilinear grid with a polar coordinate grid. The level set approach appears to be more flexible with respect to grid cell size, and more efficient in the grid computation. It also extends naturally to the construction of 3D grids, unlike the elliptic technique. The algorithm presented here effectively employs image processing tools for the boundary detection followed by a level set method for the interior grid generation. As such, the user's intervention is minimal. All computations reported below were performed on a Pentium 4 3.00 GHz PC using Matlab v.7.0.1.

The modelling of biological growth with diffeomorhpic maps: In computational anatomy [7], the relationships between brain structures within a given anatomic population (e.g., gyri and sulci in 2D brain slice images, cortical surfaces) are described via diffeomorphic transformations (one-to-one, onto, differentiable with differentiable inverse) defined over a continuum. $\boldsymbol{x} = (x_1, x_2, x_3) \rightarrow \boldsymbol{h}(\boldsymbol{x}) = (h_1(\boldsymbol{x}), h_2(\boldsymbol{x}), h_3(\boldsymbol{x})) = \boldsymbol{x} - \boldsymbol{u}(\boldsymbol{x}) \in \Omega$, where $\Omega \subset \mathbb{R}^3$ represents some component of a human brain and $\boldsymbol{u}(\boldsymbol{x})$ is the displacement field.

Diffeomorphic transformations can also be used to capture external and internal morphological changes of a growing organism. During growth, for example, a biological structure undergoes internal changes in the form of local expansions or contractions. Growth then can be described by subsequent deformations of a grid representing anatomical structures at different ages. Since biological growth exhibits significant variability among organisms in a given population, such deformations are probabilistic. This leads to the modelling of biological growth as a sequence of random transformations [3,4]. These transformations should be biologically motivated with the underlying genetic control. To represent a changing anatomy of the growing organism due to the effect of the genes we construct the biological coordinate system.

2 The "Darcyan" Biological Coordinate System

The developing organism will undergo shape and internal changes under the patterned control of a multitude of genes. For example, mouse embryonic development is controlled by 308 genes. The gene expression pattern manifests itself in the form of a spatio-temporal distribution of densities of gene products. Fig. 1 shows the regional expression of gene `Fgf8`, called the fibroblast growth factor [6], in the developing mouse embryo observed at different phases of development. Regions with different gene activities designate formative areas where elementary structural changes such as, e.g., cell division, are expected.

It seems natural to construct a coordinate system within an organism for the spatial distribution of gene activity regions and for capturing shape and internal structure changes caused by the active genes. Grenander [3] introduced the "Darcyan" coordinate system, named in honour of D'Arcy Thompson [14], so that an elementary biological event such as cell division or cell death is expressed as a point or "seed" in the organism. The "seed" is a signal for a structural change.

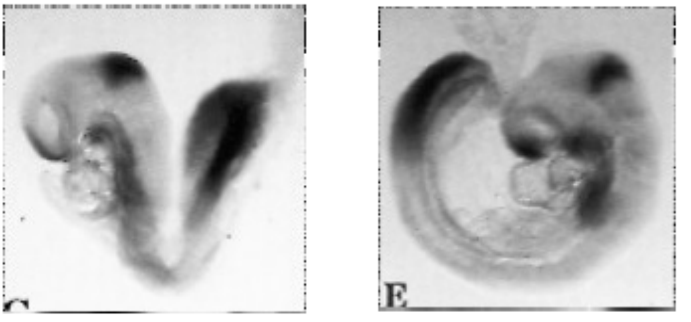

Fig. 1. Photomicrosopic images of stained embryos corresponding to the gestation periods of approximately 8 and 9 days. Reproduced with permission of the Company of Biologists.

Given an arbitrary organism occupying a region $\Omega(t_0) \in \mathbb{R}^2$ at initial time t_0 (see Fig. 2), we shall denote its intrinsic coordinate system as Ξ. All biological decisions will be made inside $\Omega(t)$ for $t \geq t_0$ in terms of the time-dependent biological coordinates $\xi = (\xi_1, \xi_2)$. As seen in Fig. 2, Ξ is a curvilinear coordinate system with ξ_1 and ξ_2 representing radial and angular level sets, respectively. Points in $\Omega(t)$ are given in absolute space coordinates $\boldsymbol{x}(\xi_1, \xi_2)$.

Overall, the biological coordinate system of the organism consists of the Cartesian coordinate system $(x_1, x_2) \in \Omega(t)$ which reflects its gross anatomy along with its boundary, and the curvilinear coordinate system $(\xi_1, \xi_2) \in \Xi$ which carries the genetic program of its development. Mathematically, the Darcyan coordinate system $\boldsymbol{x} : (\xi_1, \xi_2) \in \Xi \rightarrow (x_1, x_2) \in \Omega(t)$ is a Lagrangian coordinate system: the Lagrangian coordinates $\xi = (\xi_1, \xi_2)$ follow structural changes of the organism as it develops in time.

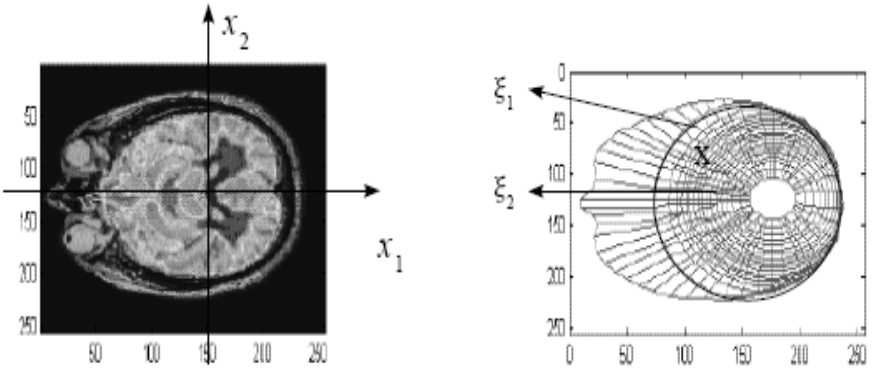

Fig. 2. A given organism $\Omega(t_0)$ and its biological coordinate system Ξ. X represents a "seed," i.e., a location of an elementary biological event.

3 Construction of the Biological Coordinate System: The Elliptic Technique

In order to design a biological coordinate system within an organism $\Omega(t) \in \mathbb{R}^2$ we impose the following requirements:

1. the distribution of grid cells is uniform
2. the coordinate curves are relatively orthogonal
3. the coordinate curves are smooth.

Grenander [3] proposed to construct the biological coordinate system by solving Poisson's equation with Dirichlet boundary conditions in $\Omega(t_0)$ by placing a unit charge – modelled by a Dirac delta function – at an arbitrary interior point $P \subset \Omega(t_0)$, i.e.

$$\Delta u = \delta_P, \qquad u|_{\partial\Omega(t_0)} = 0. \tag{1}$$

Given an image I in the form of an $m \times n$ matrix of greyscale intensity values, we select a region of interest using the Matlab Image Processing Toolbox command `roipoly` to obtain a binary image of the same size with zeros outside the region $\Omega(t_0)$ and ones inside it (see Fig. 3).

The numerical solution of Eq. (1) will produce equipotential contours of u within the X-field. We solve this boundary value by discretizing the Laplacian on an $m \times n$ lattice with integer nodal values and lattice cell size $\delta x = \delta y = 1$. We apply a simple numerical method known as the *method of successive under-relaxation* [12], with relaxation parameter $w < 1$, as follows. Starting with the initial guess for the solution, $u_{ij}^{(0)} = u^{(0)}(x_i, y_j) = 0$, $1 \le i \le m$, $1 \le j \le n$, we update its values according to the iteration scheme

$$u_{ij}^{(n)} = (1-w)u_{ij}^{(n-1)} + w\frac{1}{4}\left(u_{i+1,j}^{(n-1)} + u_{i-1,j}^{(n-1)} + u_{i,j-1}^{(n-1)} + u_{i,j+1}^{(n-1)} - \delta_{Pij}\right), \tag{2}$$

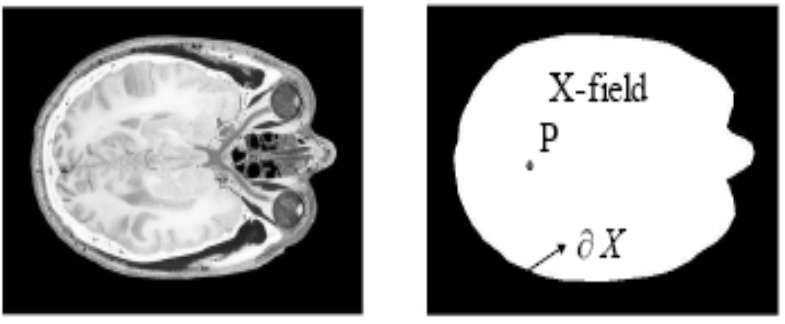

Fig. 3. An image I of a brain slice (left) and its interior (right) as a selected region of interest. P is a pole which serves as the origin of the biological coordinate system.

where $\delta_{P_{ij}} = 1$ if $(x_i, y_j) = P$ and $\delta_{P_{ij}} = 0$ otherwise. A result obtained by 2000 such iterations with the relaxation parameter $w = 0.8$ is shown in Fig. 4(a).

Note how the equipotential contours $u(x_1, x_2) = C$, i.e., radial level sets, appear concentrated in the neighbourhood of the pole P. In order that the level sets be more evenly distributed, we consider the application of a nonlinear transformation to the solution of Eq. (1). For example, in Fig. 4(b) is presented a graph of the normalized potential v given by

$$v(x_i, y_j) = (Lu)(x_i, y_j) = \frac{1}{\max_{i,j} u(x_i, y_j)} \left[1 - e^{u(x_i, y_j)}\right] \tag{3}$$

after application of the Matlab histogram equalization procedure `(histeq,250)`, where 250 is the number of discrete greyscale values in the image.

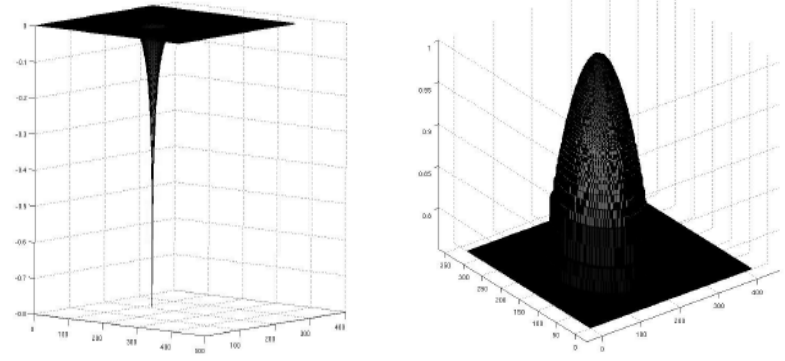

Fig. 4. (a) Graph of the potential function $u(x)$, a solution to the Dirichlet boundary value problem in Eq. (1) along with level sets. (b) Graphs of the normalized potential function $Lu(x)$, as given by Eq. (3), along with level sets.

In order to find the orthogonal angular coordinate curves, we parameterize the boundary $\partial\Omega$ by the arclength as $x(s),\ 0 \leq s \leq L$. Then let $\xi_2 = s$ and solve, for fixed ξ, the following ODE, given in vector form,

$$\frac{dx(t,\xi_2)}{dt} = \frac{\nabla v}{\parallel \nabla v \parallel}. \tag{4}$$

Here, v is the modified potential function obtained by means of some nonlinear transformation applied to the potential solution u of Eq. (1) and ∇v denotes the gradient of v at a point $x \in X \cup \partial X$ outside a neighbourhood of pole P. The system of N discretized ODEs in (4) describes the advection of N initially equidistant points on the boundary ∂X of the organism in the direction of ∇v, which is initially normal to ∂X at a boundary point x. When each of these trajectories reaches the first nonzero radial level set $u(x(t_1,\xi_2)) = C_1$ or, equivalently, $\xi_1 = t_1$, we set $\xi_1 = t_1$ on each of the N solution curves. in this fashion, we generate N angular coordinate curves that cross $N-1$ radial coordinate curves by moving the points $x(\xi_1 = t, \xi_2 = s_j)$, $1 \leq j \leq N$, in a normal direction for $\xi_1 = t_i$, $t_1 < t_2 < \cdots < t_{N-1}$.

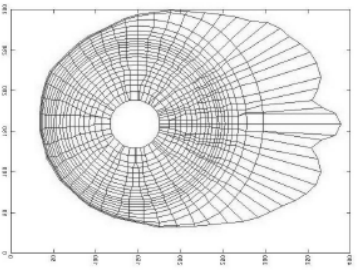

Fig. 5. The Darcyan coordinate system constructed for the interior of the brain slice of Fig. 3

Examples of such Darcyan coordinate systems constructed by this elliptic technique are shown in the right panel of Fig. 2 and in Fig. 5. The computation of the radial and angular level sets was performed on a rectangular grid of 333×418 points. For $N = 60$, the total CPU time required was 67.38 seconds. Since the positions of boundary points as computed by Eq. (4) were restricted to integer values on the grid, the trajectories of some neighbouring points, as they moved closer to the origin and therefore to one another, merged into one trajectory. One way to overcome this difficulty is to redistribute the points along the non-zero radial level sets. Also, the grid cells appeared non-uniform in size. This is not usually an issue when one is interested in tracking localized growth away from the boundary.

All in all, the resulting Darcyan grid can be improved, if needed, depending upon the user's intentions. For example, the accuracy in the approximation of the potential function solution of Eq. (1) could be increased, or the pole relocated

or the refinement of the Cartesian grid increased. Unfortunately, there is an issue regarding the Poisson method for 3D coordinate grid generation: it is not guaranteed that a trajectory passing through an interior point is unique [3].

4 Construction of the Biological Coordinate System: The Level Set Method

The level set method, introduced by Osher and Sethian [8] and described in [11], provides an alternative technique for the generation of Darcyan coordinate systems in 2D and 3D. In [10], it was shown that the level set method of the body-fitted grid generation method provides an efficient and flexible way of constructing evenly distributed, smooth exterior or interior grid lines around some closed, simply connected set X with an arbitrary boundary ∂X. However, the particular examples treated in [10] were limited to convex and nonconvex axisymmetric sets for which the radial coordinate curves tend toward a circle that smoothly collapses to a point that determines the origin of the coordinate system (Grayson-Hamilton theorem [2]). Below, we propose a level set technique that constructs a grid within an arbitrary set X.

The basic idea of this method is to view the boundary (or surface in the 3D case) of an organism as a propagating front. This front propagates inward and normal to itself with a speed law F that ensures the smooth evolution of the coordinate curves. Since a front that moves at a speed F which depends upon its curvature k and normal direction remains smooth for all times [11], the function $F(k)$ given by [10]

$$F(k) = \min(-k, F_{threshold}), \tag{5}$$

is an adequate model for our purposes. $F_{threshold}$ is needed to ensure that points with high negative curvature (i.e., belonging to nonconvex parts of the propagating boundary) do not move against the inward flow. We stress the fact that the front evolution under the speed law (5) is a geometric curve flow. The theory of front evolution [9] views the front as an interface separating two regions, and the Eulerian level set formulation of front motion [11] is usually chosen to construct a physically meaningful solution. Since the speed is determined by the intrinsic geometric properties of the front, it is natural to formulate the equations of front evolution in the following Lagrangian form,

$$x_t = F(k)\frac{y_s}{\sqrt{x_s^2 + y_s^2}}, \quad y_t = -F(k)\frac{x_s}{\sqrt{x_s^2 + y_s^2}}, \tag{6}$$

with $x(s,0) = \alpha(s)$ and $y(s,0) = \beta(s)$, $s \in [0,S]$, $t \in [0,T]$. Here $\boldsymbol{X} = (x(s,t), y(s,t))$ is the position vector of the curve, parametrized by $s \in [0,S]$. The unit normal $\boldsymbol{n}$ to the evolving front and the mean curvature k are given by

$$\boldsymbol{n} = \left(\frac{y_s}{\sqrt{x_s^2 + y_s^2}}, -\frac{x_s}{\sqrt{x_s^2 + y_s^2}}\right), \quad k = \frac{y_{ss}x_s - x_{ss}y_s}{(x_s^2 + y_s^2)^{3/2}}. \tag{7}$$

The problem of front motion in (6) is idealized when $\alpha(s)$ and $\beta(s)$ are given as smooth functions of s. In medical images, the boundaries of anatomical structures may exhibit a complex behaviour such as significant oscillations or sharp corners. Hence the initial data for the equations of motion in (6) are given in the form of an array of coordinates of boundary pixels. We are faced with two problems:

1. Extraction of the initial boundary information
2. Numerical solution of the equations of motion (6) using discrete parametrization of the front.

In order to solve these problems, we propose the following algorithm.

Algorithm for interior coordinate system generation

1. Apply an averaging filter to a given image to remove small noise (e.g., small notches, oscillations) from the boundary.
2. Convert the intensity image to a binary image using the computed global image threshold intensity level.
3. Trace an object in the binary image by specifying the coordinates of the starting boundary pixel (its value is 1) and the initial direction for the search of the neighbouring boundary pixel. The Matlab image processing procedure `bwtraceboundary` identifies boundary pixel coordinates (See Fig. 6(b)).
4. Apply a linear transformation to the pixel coordinate system to shift the origin to the middle of the image domain and plot the extracted boundary (see Fig. 6(c)).
5. Reparametrize the boundary by the arclength α – note that, by definition, $d\alpha = \sqrt{(x_s^2 + y_s^2)}ds$ – and place N nodes $\boldsymbol{X}(\alpha_1), \boldsymbol{X}(\alpha_2), \cdots, \boldsymbol{X}(\alpha_N)$ uniformly in arclength over the boundary curve (see Fig. 7(a)).
6. Initialize the time step δt so that the ratio $\delta t/\delta\alpha$, the arclength spacing between neighbouring boundary nodes, satisfies the Courant-Friedrichs-Levy condition for stability of the numerical algorithm.
7. Discretize the equations of motion (6) using central difference schemes to approximate parameter derivates at each node. Then solve the system of N unlinked ordinary differential equations with unknowns $\{\boldsymbol{X}(\alpha_i(\Delta t), \Delta t)\}_{j=1}^{N}$ using a second-order Heun's method.

Fig. 6. (a) Given image, (b) automatic boundary detection, (c) extracted boundary in absolute space

8. Redistribute the nodes along a new radial curve to maintain their equal arclength spacing and thus to avoid the merging of trajectories of nodal points.
9. Update the values for the time step and the arclength spacing, Δt and $\Delta\alpha$, respectively.
10. Repeat steps (7), (8) and (9) until the average length of trajectories of nodal points leaving the initial boundary becomes greater or equal to the initial arclength spaceing multiplied by the parameter $coef \leq 1$, which controls the uniformity of grid cell size and depends upon the user's preference. Record and display the position of obtained radial lines as well as nodal trajectories (since they are angular curves).
11. Reinitialize the radial line obtained and apply steps (7)-(10) to the new initial curve until it is possible to control the stability of the numerical scheme (see Fig. 7(b)).

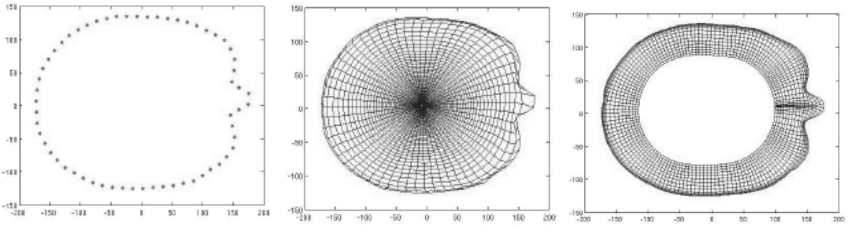

Fig. 7. (a) Nodal distribution along the intial boundary, $N = 60$. (b) Interior grid of size 77×60. (c) Generation of interior grid without transversal adjustment.

Some comments on the results of the algorithm 1. The interior coordinate system appears well-structured at a cost of loss of orthogonality of coordinate curves. For initially nonconvex shapes, it is not always possible to compute the advection of N nodes of radial lines in their normal direction (Step 7) without nodal redistribution (Step 8) as time progresses. The transverse lines (nodel trajectories) can come together as shown in Fig. 7(c) and cause computational problems (division by zero). In order to avoid this difficulty, we have performed transversal adjustment according to the length of an obtained radial line. Other techniques of nodal redistribution are discussed in [10].

2. As an initially nonconvex closed curve propagates inward under the curvature flow defined by (5) and (6), it will not necessarily collapse to a convex shape (see Fig. 8(a)). Moreover, the arclength spacing between neighbouring nodes decreases with time, causing the time step to decrease, thereby making further computations very expensive.

3. In particular, small variations in the computed curvature will grow unconditionally when the arclength spacing becomes on the order of 10^{-2}. To prevent the development of oscillations in the moving curve, some boundary smoothing techniques can be used. A simpler solution to this computational problem would be to terminate the propagation of the boundary as soon as its length starts

to grow, followed by a smooth patching of the resultant curvilinear coordinate curves with polar coordinate curves (see Fig. 8(b)). To achieve a transition to the polar grid, we apply an angle-preserving transformation to the terminating radial curve that changes the length of the radius-vector tracing its N nodes $\boldsymbol{R} = \boldsymbol{X}(\alpha) - \boldsymbol{X}_{origin}$ to the radius of a disk while preserving its angle with respect to the abscissa axis x_1. Thus, the angular lines will "flow" to the origin of the Darcyan coordinate system, $\boldsymbol{X}_{origin}$ hat can easily be computed as the middle point of the terminating radial curve diamer (the maximum Euclidean distance between points of the curve). In general, this transition cannot guarantee the smoothess of angular coordinate curves since they may enter the terminating radial curve at angles that are different from the ones formed by the radius-vector R and the x_1-axis. It may not be necessary to "close off" the constructed interior grid with the polar grid when one is interested in overall effects of growth on structural and shape changes. However, if it is a localized growth in the neighbourhood of the origin that causes shape changes then the *complete* interior coordinate system is needed.

All in all, the level set-based algorithm provides the most natural way to generate an intrinsic coordinate system within the organism together with its boundary since it allows the coordinate curves to align with its shape curves. It is a biologically meaningful coordinate system in the sense that the genetic program of the organism's development, expressed in terms of the Darcyan ξ_1 and ξ_2 coordinates, which in turn designate the locations of biological decisions (active genes) are independent of the absolute or physical space. The constructed Darcyan coordinate system provides a computational grid $\boldsymbol{X}(\xi_1, \xi_2)$, $1 \leq i \leq M$, $1 \leq j \leq N$, that deforms in time as the organism develops, thus reflecting its gross anatomical changes.

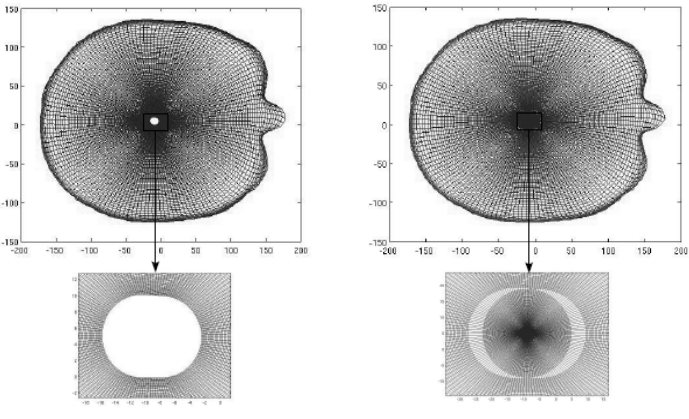

Fig. 8. (a) Curvilinear coordinate system and a close-up view of the neighbourhood of the terminating radial line. (b) Patching of the curvilinear system with a polar coordinate system. Image size: 150×211.

4.1 More Examples of 2D Darcyan Coordinate Systems

We have tested our level-set algorithm for Darcyan coordinate system generation, described above, on other biological shapes. In Fig. 9(a) is shown a snapshot of a growing snapdragon petal lobe [13]. The coordinate system within the petal lobe (see Fig. 9(b)) was obtained with the grid parameters $F_{threshold} = -|\bar{k}(t)|$, where $\bar{k}(t) = (1/N)\sum_{i=1}^{N} k(\delta\alpha_i, t)$ is the mean curvature of the propagating boundary, $N = 150$ is the number of angular coordinate curves, $coef = 0.6$ is the grid cell size control parameter, and the ratio $\Delta t/\Delta\alpha = 0.8$ ensures the stability of the numerical scheme. Note that with this value of the parameter $coef$ we achieve a relatively uniform grid with only 37 radial lines. The value of $coef$ controls the density of the field lines: the smaller it is, the denser the field lines are. Computation of the grid required about 1 min of CPU time.

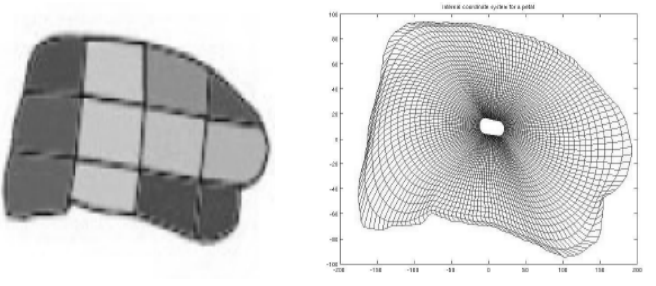

Fig. 9. (a) Snapdragon petal lobe (courtesy of A.-G. Rolland-Lagan, J.A. Bangham, E. Coen). (b) The associated Darcyan coordinate system as an interior grid of size 150×37.

For a more complex shape of a mouse embryo [1] given in Fig. 10(a), we chose the number of angular lines to be $N = 300$, $coef = 1.0$ and $\Delta t/\Delta\alpha = 0.3$. The pointy mouse tail creates a localized high curvature variation in the embryo shape, presenting a major difficulty in handling nodal trajectories near the initial boundary. According to our algorithm, radial curves are recorded at time $\Delta T = \sum_{i=1}^{M} \Delta t_i$, when the average length of these trajectories reaches the arclength spacing of the previous radial curves. However, if we connect them with line segments, then these line segments will intersect.

Therefore, unlike the cases for the brain slice and the snapdragon petal, we record and display nodal trajectories at each time step $\Delta t = 0.3\Delta\alpha$ until the total variation of the moving radial line has significantly decreased. In this way, we obtain a more accurate behaviour of angular curves near the initial boundary. Representing the initial boundary with $N = 300$ notes yields a finer grid (see Fig. 10(b)), thus allowing us to capture the geometry at a finer scale, such as the shapes of developing toes.

The examples presented above demonstrate the flexibility of the level set-based algorithm in grid design and its ability to handle corners and cusps in the initial boundary. It is also an efficient tool for interior grid generation. The CPU

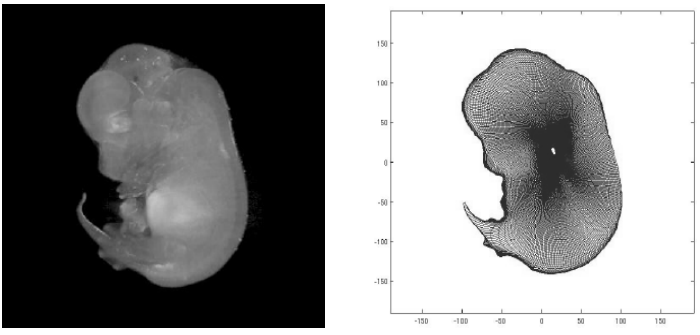

Fig. 10. (a) A mouse embryo from the online mouse development atlas at `http://genex.hgu.mrc.ac.uk/Atlas/intro.html`. (b) Darcyan coordinate system of this embryo as an interior grid of size 300×125.

time for the 60×77 grid computation inside the brain slice (Fig. 9(b)) was 55.29 sec, as compared to the 67.38 sec required for the 60×60 grid (Fig. 7) using the elliptic technique.

5 An Application of the Darcyan Coordinate System to Model Biological Growth

The construction of a Darcyan coordinate system representing the domain of a biological system allows us pursue one of the goals of computational anatomy outlined in Section 1, namely to simulate the growth of the system. This can be accomplished provided that the growth properties (e.g., growth rate in space and time) are known. In Fig. 11 is presented a synthetic example of a localized radial growth within the brain slice of Fig. 6(a). There is local expansion in the active gene zone and the deformation effects decays away from the zone. As a result, there is no visible change to the boundary. With the development of the organism, its Darcyan coordinate system/grid deforms and captures the nature of localized growth. It is easily seen from Fig. 11 that the amplitude of localized growth is independent of direction.

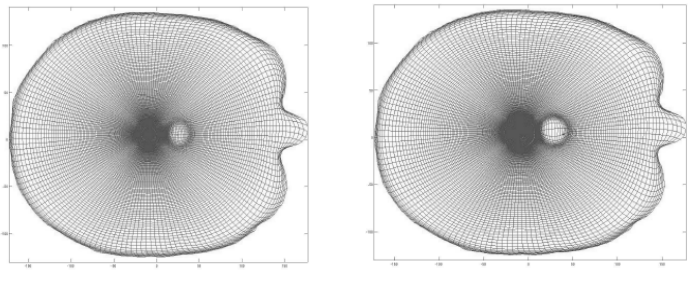

Fig. 11. Time-dependent deformations of the brain-slice Darcyan coordinate system of Fig. 6(a) that reflect localized radial growth effect on the internal structure

The Darcyan grid provides a computational domain for the application of diffeomorphic transformations that are defined by biological parameters such as amplitude of growth (possibly direction-dependent) and space- and time-dependent growth rates. As such, biological growth is modelled as a diffeomorphic flow. The deformed interior grid of the developing brain shown in Fig. 11 is a realization of a diffeomorphic flow in time applied to the initial Darcyan coordinate system of the brain slice in Fig. 8(b). This is one result of our experimental studies of the mathematical model of biological growth introduced by Grenander [3,4], further discussion of which is beyond the scope of this paper.

6 Future Research Directions

The algorithm for 2D Darcyan coordinate system generation presented here requires further exploration in the case of significantly oscillating shapes (e.g. a "dumbbell" region). In such cases, the propagating front may not collapse to a single radial curve, requiring that the initial organism domain be segmented into two or more disjoint subdomains.

The flexibility and robustness of the level set approach for Darcyan grid generation is an asset when constructing 3D grids. The control of the distances between transversal trajectories can be devised automatically, thus ensuring their separation at each time increment. According to [10], the level set technique of 2D grid generation extends in a straightforward manner to 3D. In the volumetric case, the Eulerian formulation of the equations of front motion is preferable. According to the Eulerian approach, the zero level set surface of a four-dimensional moving surface defines the position of the front. The Lagrangian method based on discrete parameterization of the moving surface would be extremely expensive to realize, requiring a redistribution of surface nodes, tracking nodal trajectories and a small time step for the stability of the numerical solution. We are further developing the level set-based algorithm to be applicable to 3D Darcyan grid construction.

Acknowledgements

This research was supported in part by the Natural Sciences and Engineering Research Council of Canada (NSERC) in the form of a Discovery Grant (ERV) and a Postgraduate Scholarship (NP), which are hereby gratefully acknowedged.

References

1. Davidson, D., Bard, J., Kaufman, M., Baldock, R.A.: The Mouse Atlas Database: A Community Resource for Mouse Development. Trends in Genetics 17, 49–51 (2001)
2. Grayson, M.: The heat equation shrinks embedded plane curves to round points. J. Diff. Geom. 26, 285–314 (1987)

3. Grenander, U.: On the mathematics of biological growth (unpublished manuscript) (2005)
4. Grenander, U.: Mathematics in biology, PowerPoint presentation to Grand Mathematical Challenges in Medical Imaging workshop, University of Waterloo (October 2005)
5. Knupp, P., Steinberg, A.: Fundamentals of grid generation. CRC Press, New York (1993)
6. Lee, S.M., Danielian, P.S., Fritzch, B., McMahon, A.P.: Evidence that FGF8 signaling from the midbrain-hindbrain junction regulates growth and polarity in the developing midbrain. Development 124(5), 959–969 (1997)
7. Miller, M.I., Grenander, U.: Computational anatomy: An emerging discipline. Quart. Appl. Math. 4 (1998)
8. Osher, S., Sethian, J.A.: Fronts propagating with curvature-dependent speed: Algorithms based on Hamilton-Jacobi formulation. J. Comp. Phys. 79, 12–49 (1988)
9. Sethian, J.: An Analysis of Frame Propagation, Ph.D. dissertation, Dept. of Mathematics, University of California, Berkeley, CA (1982)
10. Sethian, J.: Curvature flow and entropy conditions applied to grid generation. J. Comp. Phys. 115, 440–454 (1994)
11. Sethian, J.: Level Set Methods: Evolving Interfaces in Geometry, Fluid Mechanics. Computer Vision and Materials Science. Cambridge University Press, Cambridge (1996)
12. Press, W.H., Flannery, B.P., Teukolsky, S.A., Vetterling, W.T.: Numerical Recipes in C: The Art of Scientific Computing. Cambridge University Press, Cambridge (1988)
13. Rolland-Lagan, A.-G., Bangham, J.A., Coen, E.: Growth dynamics underlying petal shape and asymmetry. Letters to Nature 422, 161–163 (2003)
14. Thompson, D.: On Growth and Form. Cambridge University Press, Cambridge (reprint of 1917 edition) (1961)